https://doi.org/10.15302/frontphys.2025.044203

RESEARCH ARTICLE

Photonic biosensing through cascade-coupled Su-Schrieffer-Heeger boundary modes

Yang Liu[1], Jian-Hua Jiang[2, 3, 4, 1, †]

[1]School of Physical Science and Technology & Collaborative Innovation Center of Suzhou Nano Science and Technology, Soochow University, Suzhou 215006, China

[2]School of Biomedical Engineering, Division of Life Sciences and Medicine, University of Science and Technology of China, Hefei 230026, China

[3]Suzhou Institute for Advanced Research, University of Science and Technology of China, Suzhou 215123, China

[4]Deparment of Modern Physics, School of Physical Sciences, University of Science and Technology of China, Hefei 230026, China

Corresponding author. E-mail: [†]jhjiang3@ustc.edu.cn

Received December 25, 2024; accepted March 4, 2025

Supporting Information

Note A: The robustness of edge modes architected by topology domain wall

The edge modes engineered by a couple of nontrivial and trivial SSH arrays, in a sense, are well immune to the manufactured defects. Here, we introduce three circular silicon defects with the identical radius r to act the manufactured defects, and then perform how the edge modes are robust to them via the transmission spectrum. As a comparison, we rebuild a PhC strip based on the topological nontrivial SSH cells but remove three silicon pillars to construct the hole defects [see Fig. S1(a)]. This configuration supports three hole modes [see red curves in Fig. S1(b)] that play the in-gap transport channels akin to the edge modes. Therefore, the hole-version PhC strip can also offer a comparable transmission spectrum.

In Fig. S1(c), we give the transmission spectra simulated by COMSOL, and label the three edge (hole) modes as E0 (H0), E1 (H1), and E2 (H2). The transmission spectra of edge-version and hole-version strips are figured in the same-scale frequency axis for a better comparison in visual. One can clearly observe that the transmission peaks of edge modes are more robust in the frequency domain than those of hole modes. Even when the radius of the silicon defects increases to 0.1a, the transmission peaks of the edge modes are redshifted by only 0.05c/a on average. Meanwhile, in the hole version, these peaks are redshifted by about 0.1c/a that doubles those in the edge-version PhC strip. Further enlarging the silicon defects, it is easy to infer that these hole modes will be unobserved due to falling into the bulk states, while the edge modes with robustness can circumvent this. The stability of edge modes in frequency domain is crucial to the functionality of optical biosensors. It is worth noting that Fig. S1(c) may lead one to wrongly conclude that the transmittances of hole channels are more robust to the manufactured defects. We need to clarify that the edge modes here are asymmetric (see the intensity peaks slightly deviating the interfaces in Fig. 3), while the applied silicon defects keep the mirror symmetry that significantly impact the transmittance of E1 and E2 peaks. As a contrast, the hole modes maintain their near-mirror symmetry under the silicon defects, which is conducive to keep the configurations of H1 and H2 peaks. In fact, the probability of mirror-symmetric manufactured defects is extremely low, thus the above conclusion about the transmittance is unreliable and useless. In addition,

from Fig. S1(c), one can see that the transmission peaks of edge modes are thinner than those of hole modes, which means that transmission signals based on topological edge modes are better in resolvability. In summary, we verify the robustness of the topological edge modes and exhibit their excellent performance in optical biosensors.

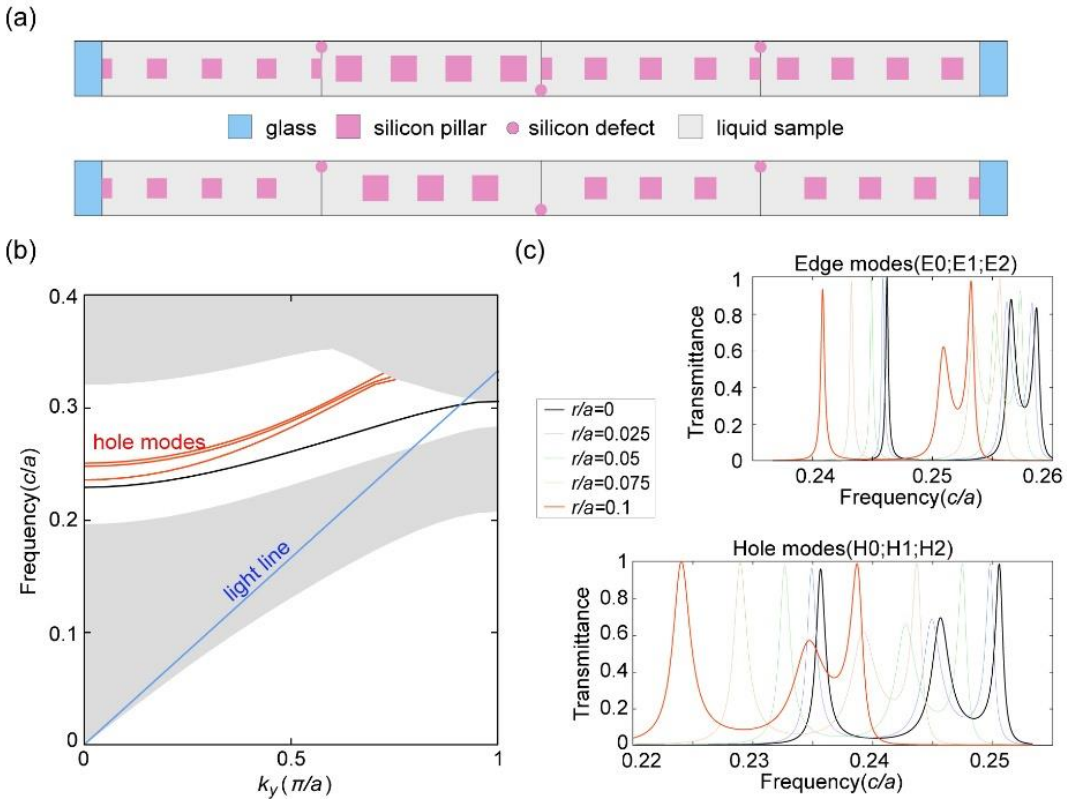

Fig. S1 (a) Schematics of the edge-version and hole-version PhC strips with silicon defects. **(b)** The band diagram of the hole-version PhC strip. Red curves denote the hole modes. **(c)** The responses of transmission spectra to silicon defects. r means the radius of a single silicon defect.

Note B: Mode couplings and transmission spectra

According to the wave functions for E0, E1, and E2 modes shown in the main text Fig. 2(c), we can infer the following Hamiltonian corresponding to the case with $k_y = 0$:

$$H = \begin{pmatrix} \varepsilon_L & t_{LC} & t_{LR} \\ t_{LC} & \varepsilon_C & t_{CR} \\ t_{LR} & t_{LC} & \varepsilon_R \end{pmatrix}. \quad (B1)$$

ε_i means the eigen frequency of i interface mode. t_{ij} denotes the coupling between i and j interface modes. For our PhC strip setup, the fitting parameters are $\varepsilon_L = 0.2571$, $\varepsilon_C = 0.2485$, $\varepsilon_R = 0.2556$, $t_{LC} = -0.002$, $t_{CR} = 0.004$, and $t_{LR} = -0.0005$ in units of c/a. The solved three eigenvalues are $\varepsilon_{E0} = 0.2465c/a$, $\varepsilon_{E1} = 0.2561c/a$, and $\varepsilon_{E2} = 0.2586c/a$, which is close to the frequencies for E0, E1, and E2 modes in main text. And then we picture their eigenvectors in Fig. S2(a). It is found that they are in good agreement with the major electric fields of three interfaces in Fig. 2(c). Therefore, our fitting parameters are reasonable.

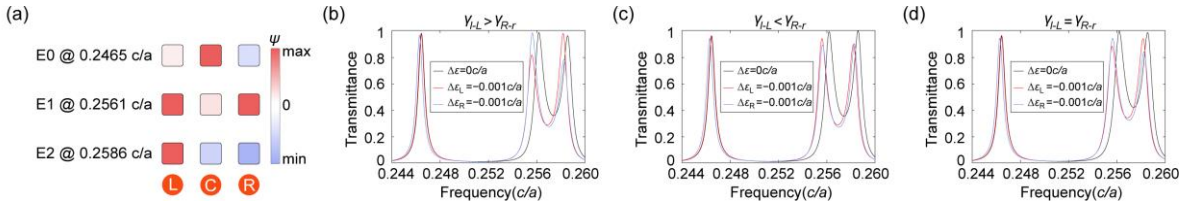

Fig. S2 (a) Eigen wavefunctions of three-mode coupling mode. **(b-d)** Calculated transmission spectra via Landauer-Büttiker formulation. In (b), $\gamma_{l-L} = 0.001c/a,\ \gamma_{R-r} = 0.0008c/a$. In (c), $\gamma_{l-L} = 0.0008c/a,\ \gamma_{R-r} = 0.001c/a$. In (d), $\gamma_{l-L} = 0.001c/a,\ \gamma_{R-r} = 0.001c/a$.

To understand the photonic transport through our PhC biosensor, we employ the Landauer-Büttiker theory [1]. In this theory, the transmission spectrum is given by

$$T(\varepsilon) = Tr(\Gamma_L G_r \Gamma_R G_a). \tag{B2}$$

Here, matrix Γ_L describes the scattering rates from the photon continuum in left glass to the central PhC strip. Matrix Γ_R describes the scattering rates from PhC strip into the photon continuum in the right glass. Green functions G_r and G_a are the retarded and advanced Green functions. And they are connected by the relation, $G_a = G_r^{\dagger}$. The retarded Geen function takes the following form:

$$G_r = \left[\varepsilon I - H + \frac{i}{2}(\Gamma_L + \Gamma_R)\right]^{-1}. \tag{B3}$$

Since, the central PhC strip can be considered a three-mode coupling model (Eq. B1), scattering matrixes Γ_L and Γ_R can be expressed by three scattering rates that three modes scatter into the left and right glass. Here, the scattering matrix takes the form,

$$\Gamma_{L(R)} = \begin{pmatrix} \gamma_{l-L(L-r)} & 0 & 0 \\ 0 & \gamma_{l-C(C-r)} & 0 \\ 0 & 0 & \gamma_{l-R(R-r)} \end{pmatrix}. \tag{B4}$$

For simplicity, the scattering rates are set as constants: $\gamma_{l-L} = 0.001$, $\gamma_{l-C} = 0.0003$, $\gamma_{l-R} = 0$, $\gamma_{L-r} = 0$, $\gamma_{C-r} = 0.0003$, and $\gamma_{R-r} = 0.0008$ in units of c/a. l and r denote the left and right glasses. The special relation, $\gamma_{l-L} > \gamma_{R-r}$, is available. To simulate the accumulation of protein-binding layers in the main text, we reduce the onsite energy of the corresponding modes by $0.001c/a$. And the results are shown in Fig. S2(b). Since there is a fitting bias, the transmittances of E1 and E2 peaks are higher than those in reference spectrum [main text Fig. 4(a)]. However, we can still analyze the effects of binding configurations on the transmittance differences between E1 and E2 peaks. For the case with $\Delta\varepsilon_L = -0.001$, compared to the reference ($\Delta\varepsilon = 0$), one can conclude that L-type binding causes a lower E1 peak and a higher E2 peak, while R-type binding works reversely. These conclusions are consistent with those in the main text. Then, we reverse the scattering rate relation via $\gamma_{l-L} = 0.0008c/a$ and $\gamma_{R-r} = 0.001c/a$. The calculated transmission spectra are shown in Fig. S2(c). There is no considerable transmittance difference between E1 and E2 peaks. It seems that the influence of asymmetric scattering rates ($\gamma_{l-L} < \gamma_{R-r}$) is restrained. Cases with $\Delta\varepsilon_L = -0.001$ and $\Delta\varepsilon_R = -0.001$ are no longer distinguishable. To find the enforcer of restraint, we set $\gamma_{l-L} = \gamma_{R-r} = 0.001c/a$, and the results are shown in Fig. S2(d). Obviously, the asymmetry of three-mode coupling model itself causes an effect similar to the occasion dominated by $\gamma_{l-L} > \gamma_{R-r}$, but to a lesser extent. Therefore, the asymmetric scattering rates, mode couplings, and mode hybridizations jointly

give rise to the opposite variations on the transmittances of E1 and E2 peaks, and the distinction between L- and R-type protein bindings.

References

1. M. Büttiker, Y. Imry, R. Landauer, and S. Pinhas, Generalized many-channel conductance formula with application to small rings, *Phys. Rev. B* 31, 6207 (1985)